MNRAS 000, 1–11 (2015) Preprint 21 July 2022 Compiled using MNRAS LATEX style file v3.0

A broad survey of spectro-temporal properties from FRB20121102A

Mohammed A. Chamma[1]★ and Martin Houde,[1]†
[1]Department of Physics and Astronomy, The University of Western Ontario, 1151 Richmond Street, London, Ontario N6A 3K7, Canada

21 July 2022

ABSTRACT

We survey the spectro-temporal properties of fast radio bursts from FRB20121102A across a wide range of frequencies in an effort to study if all the bursts from a single source obey the same relationships or if multiple classes emerge. We investigate 138 bursts from FRB20121102A spanning frequencies 1-7.5GHz, durations of <1ms-10ms, and low and high energy bursts. We find from our sample of bursts from FRB20121102A a strong agreement with the inverse relationship between sub-burst slope and duration and with other predictions made by the relativistic dynamical model introduced by Rajabi et al. 2020 and for which Chamma et al. 2021 found agreement with across three different sources. For this sample of bursts, we find that the sub-burst slope as well as the drift rate are quadratic with frequency, that both these quantities are inversely proportional to the duration as well as finding that the duration decreases with increasing frequency. We also find a correlation between the bandwidth and sub-burst duration, and conversely with the sub-burst slope that has not been discussed thus far. No significant group of bursts in this sample deviated from these relationships. This study demonstrates the consistent existence of a relationship between the spectro-temporal properties of bursts from an FRB source regardless of the frequency, energy, or duration of the burst observed.

Key words: fast-radio-burst – dynamical – relativistic

1 INTRODUCTION

Fast radio bursts (FRBs) are short and intense pulses of radiation whose emission mechanism eludes understanding despite a multitude of theoretical models and many recent observational efforts. Observationally, the originating environments, energy distributions, polarization properties, and activity cycles of FRB sources have been investigated with each new study often adding a new unexpected characteristic (Petroff et al. 2022). Theoretical explanations for FRBs center around extreme environments such as magnetars where large numbers of particles in a plasma state emit coherently (Lyubarsky 2021). This flurry of activity around FRBs has revealed significant challenges in understanding this phenomena and in constraining the possible explanations.

Many of the observational characteristics of FRBs vary dramatically from source to source, making it unclear which features are arising due to the emission mechanism, the environment, or propagation effects. The spectral luminosities of FRB sources spans several orders of magnitude and the durations of bursts can range from the tens of nanoseconds to the tens of milliseconds (Nimmo et al. 2021). The polarization properties of FRBs vary as well; for example in FRB20121102A bursts have a constant polarization across their duration (Michilli et al. 2018), whereas in FRB20180301A the polarization angle of some bursts show diverse behaviours (Luo et al. 2020). In FRB20190520B, the range of rotation measures (RMs) observed are the largest observed for any type of astrophysical source studied, including other FRB sources (Anna-Thomas et al. 2022). These characteristics of FRB sources complicate our understanding and are likely due to an overlap of multiple different phenomena.

One avenue for understanding the emission mechanism of FRBs is to study the spectro-temporal properties of bursts, which has revealed several relationships that are common from burst to burst and even from source to source. Among these quantities, which include the bandwidth, duration, and central frequency, are the drift rate and the similar but distinct sub-burst slope or intra-burst drift[1]. The drift rate refers to the change in frequency of multiple resolved sub-bursts within a single waterfall, and the tendency for later sub-bursts to arrive at lower frequencies is called the "sad trombone" effect. The sub-burst slope on the other hand refers to the change in frequency with time within a single sub-burst or pulse. Hessels et al. (2019) studied bursts from FRB20121102A and the relationship between their frequency and the drift rate of multiple resolved sub-bursts, finding that the drift rate increased with frequency. This relationship appeared to be linear (Josephy et al. 2019). In the relativistic dynamical model proposed by Rajabi et al. (2020), an inverse relationship was predicted between a sub-burst's slope and its duration and agreed with measurements made for a sample of bursts from FRB20121102A. This relationship was further explored in Chamma et al. (2021) where bursts analysed from three repeater sources (FRB20180916B and FRB20180814 in addition to FRB20121102A) also had sub-burst slopes that varied inversely with duration, indicating that the same relationship could describe the features of bursts from different sources. The model in Rajabi et al. (2020) also predicted a quadratic

★ E-mail: mchamma@uwo.ca
† E-mail: mhoude2@uwo.ca

[1] The 'sub-burst slope' terminology was used in Chamma et al. (2021) while 'intra-burst drift' was used in Jahns et al. (2022). Both terms describe the same measurement and we will use 'sub-burst slope' hereafter.

relationship between the sub-burst slope and the frequency, and some evidence of this can be seen in various datasets as plotted in Fig. 8 of Wang et al. (2022). Jahns et al. (2022) studied over 800 bursts from FRB20121102A in the 1.1-1.7 GHz band and also found the sub-burst slope to be inversely proportional to duration. In addition they compared the sub-burst slope to a dozen drift rates and found that the drift rates were larger but seemed to extend the same trend with the duration as the sub-burst slopes do (Jahns et al. 2022). This behaviour for drift rates and sub-burst slopes obeying similar or identical relationships is possible within the relativistic dynamical model when groups of sub-bursts are emitted at roughly the same time (Sec. 3.1 of Chamma et al. 2021; Rajabi et al. 2020). Given these recent discoveries it is fruitful to study the spectro-temporal features of bursts in order to better characterize these relationships, to find their limitations, and to find possible commonalities between sources that will contribute to our understanding of the FRB emission mechanism.

In this work we investigate if the same spectro-temporal relationships, such as the relationship between the sub-burst slope and the duration, are followed for a large and diverse sample of bursts from a single source as this will indicate if bursts from a single source can be differentiated based on the spectro-temporal relationships they obey as well as the robustness of these relationships. To this end we collect bursts from multiple observational studies of the repeating source FRB20121102A, one of the best observed repeaters with bursts that cover a wide range of frequencies and durations, and measure their spectro-temporal properties. Our measurements include the central frequency, the sub-burst slope, the sad-trombone drift rate (when applicable), and the duration of every burst, and we investigate the relationships between these quantities, as well if a single relationship is sufficient to describe the data or if deviations exist.

The following sections will describe the bursts sampled for this study, the methodology for measuring the spectro-temporal properties of bursts, and the relationships observed between these quantities.

2 SAMPLED BURSTS FROM FRB20121102A

We list here the observations used and the properties of the bursts sampled for our study.

Michilli et al. (2018) observed 16 bursts from FRB20121102A using the Arecibo observatory in a band that spanned 4.1-4.9 GHz. We use all the bursts they observed and seperated the components of three of their bursts (M9, M10, and M13) for a total of 19 single pulses. The durations of these bursts as measured by their FWHM and excluding the bursts whose components we have separated range from 0.03 ms to 1.36 ms (Michilli et al. 2018).

Gajjar et al. (2018) observed 21 bursts from FRB20121102A using the Green Bank Telescope in a band of 4-8 GHz all of which were 100% linearly polarized and no circular polarization. Of these observations we exclude 5 due to their low SNR and split three of their bursts (11A, 12A, and 12B) for a total of 21 single pulses, with durations that range 0.18 to 1.74 ms (Gajjar et al. 2018).

Oostrum et al. (2020) observed 30 bursts from FRB20121102A using the WSRT/Apertif telescope in a band spanning 1250-1450 MHz (and 1220 to 1520 MHz for one burst) with much lower levels of linear polarization than observed at higher frequencies. We use 24 of these bursts with the remaining six excluded due to low SNR, and all bursts from this dataset were single pulses. The durations of these bursts, as measured by a top hat pulse with an equivalent integrated flux density, spans 1.6 to 8.2 ms (Oostrum et al. 2020).

Aggarwal et al. (2021) searched data collected by Gourdji et al. (2019) using the Arecibo telescope in a band spanning 800 MHz (that was effectively cut to around 680 MHz due to noise at the bottom of the band) and centered around 1375 MHz and, including the 41 bursts found by Gourdji et al. (2019), found a total of 133 bursts in three hours of data. Notably, almost all of these bursts occur above 1300 MHz. Of these bursts we exclude almost half due to a low SNR and separate 6 into single pulses for a total of 63 bursts. The durations of the bursts used span 1.16 ms to 17.16 ms based on the FWHM obtained from the burst autocorrelation (see Section 3).

Li et al. (2021) used the FAST telescope to detect 1652 bursts in about 60 hours of data over 47 days in a band spanning 1000 to 1500 MHz. These bursts followed a bimodal energy distribution with peaks around $10^{37.8}$ and $10^{38.6}$ erg as well as a bimodal wait time distribution with peaks at around 3.4 ms and 70 s. Aggarwal (2021) argued that the bimodality in the energy distribution is due to the burst energies being estimated using the center frequency instead of the bandwidth, where, due to the band-limited and Gaussian-like nature of FRBs, the bandwidth should be used instead. Using the bandwidths found by Li et al. (2021), Aggarwal (2021) calculated the burst energies and found that they did not show any bimodality, suggesting that the different energy distributions seen thus far are due to a bias introduced by limited observing bands. Jahns et al. (2022) found only a weak bimodality in the burst energy distribution in their sample of 849 bursts and could not confirm the result of Li et al. (2021). Nonetheless, in order to investigate if these differing properties correspond to different spectro-temporal features we sampled 20 bursts from both peaks (10 each) of the energy distribution reported by Li et al. (2021) by filtering their list of bursts to those with estimated energies between $10^{37.7}$ and $10^{37.8}$ erg for the first peak and $10^{38.6}$ and $10^{38.7}$ erg for the second peak. To select bursts with high enough SNR for a good measurement we additionally filter bursts from the first peak that have a peak flux greater than 10 mJy and greater than 100 mJy from the second peak. We also sampled bursts from the two peaks of the wait-time distribution, filtering for bursts with wait-times between 4 ms to 6 ms and with a peak flux above 40 mJy, and wait-times between 63 s to 100 s above 100 mJy. This yielded 11 and 13 bursts from each peak, respectively, for an additional 24 bursts. We also sampled a single long duration burst found, as the bursts in this dataset are among the longest ever observed. Of this sample, several more were excluded due to an SNR that was still too low to obtain measurements and many of the short waittime bursts were split into multiple components, which finally resulted in a total of 42 single pulses. The bursts used span a frequency range of 1080-1430 MHz and their FWHM durations span 0.56-15.43 ms.

The sample of bursts analysed in this study total 169 and broadly represent all the types of bursts that have been observed from FRB20121102A, spanning frequencies ranging from 1080 MHz to 7.4 GHz and durations from less than 1 ms to about and greater than 10 ms. Figure 1 shows a distribution of the frequencies and durations of the bursts used in our sample.

3 METHODS AND ANALYSIS

This section will describe how the burst waterfalls are loaded and their spectro-temporal properties measured via 2D autocorrelations of the waterfall (Hessels et al. 2019; Chamma et al. 2021), as well as the dispersion measure (DM) ranges used for the measurements, and how measurements are reviewed and validated. We also describe a graphical user interface (GUI) we developed to aid in the mea-

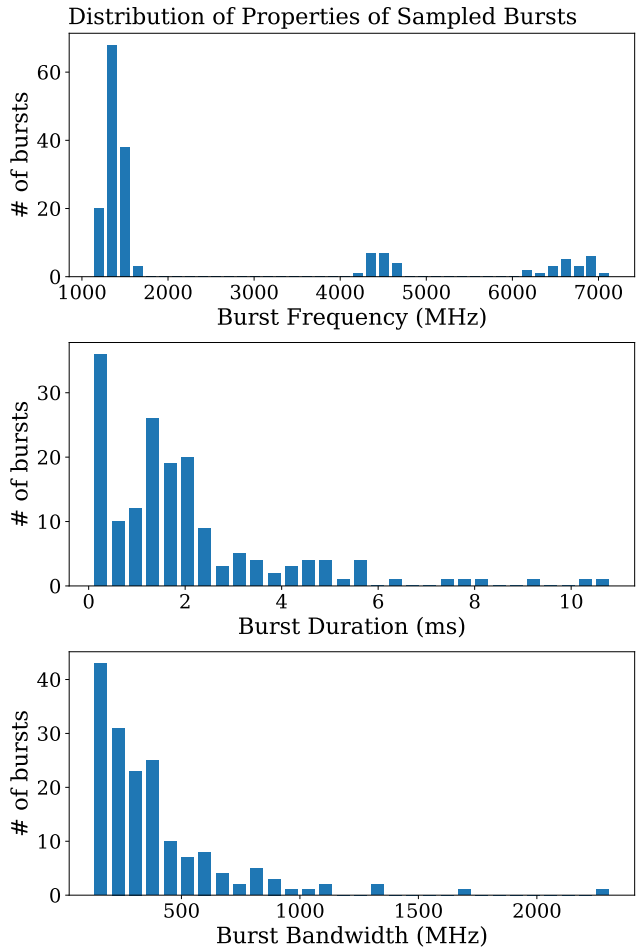

Figure 1. Histograms of the bursts sampled for this study showing the frequency (top), sub-burst durations (middle), and burst bandwidth (bottom).

surement of burst properties that is easily extensible and publicly available.

The FRB observations described in Section 2 were obtained from the authors of their respective publications and we pre-process them in order to increase signal-to-noise (S/N), remove radio frequency interference (RFI), and/or crop bursts before performing measurements. FRB waterfall data is available in various formats and the formats of the data used here include `filterbank` and `PSRFITS` files, which were loaded using the PyPulse[2] and Your[3] software packages before being stored as 2D Python `numpy` arrays. The waterfalls of bursts from Michilli et al. (2018) were provided via an ASCII dump, dedispersed, and are at frequency and time resolutions of 1.5625 MHz and 0.01024 ms, respectively, with 512 frequency channels and 512 time samples (ie. with dimensions 512 x 512). Burst waterfalls from Gajjar et al. (2018) were available dedispersed in `PSRFITS` format at a resolution of 183 kHz and 0.01024 ms with 19456 frequency channels and 2048 time samples, which we subsampled in frequency by a factor of 8 to obtain 2432 frequency channels at a resolution of 1.464 MHz. These were then stored in arrays of size 1690 x 2048 to exclude masked channels present at the bottom of the band. Waterfalls from Oostrum et al. (2020) were obtained un-dedispersed in the `PSRFITS` format with resolutions of about 0.195 MHz and 0.04096 ms with size 1024 x 25000 channels, which we dedispersed to each burst's reported DM and downsampled by a factor of 8 to resolutions of 1.5625 MHz and 0.32768 ms. These waterfalls were then centered and cropped to be stored at a size of 128 x 200 channels. In addition, before downsampling we applied both a spectral kurtosis and Savitzky-Golay filter (SK-SG filter; Agarwal et al. 2020; Nita et al. 2016) that is available via the Your package to mask channels with high RFI. The waterfall data from Aggarwal et al. (2021) are provided in long duration filterbank files with a list of candidate timestamps, and the Burstfit[4] package is used to dedisperse the data to each burst's DM and select a 0.1 s long waterfall around the burst. These waterfalls are then saved as arrays of size 64 x 1220 at resolutions of 12.5 MHz and 0.08192 ms, respectively. Data from Li et al. (2021) were obtained via correspondence and consisted of PSRFITS files for each burst. We load these with Your at a size of 4096 x 131072 channels and resolutions of 122 kHz and 0.098304 ms and then filter them with the SK-SG filter. We then dedisperse each waterfwall to the reported burst DM, subsample to 256 frequency channels, center about the time channel with the peak frequency-averaged intensity and crop to an array of size of 256 x 1000 with resolutions of 1.952 MHz and 0.098304 ms. All the bursts in this study are preprocessed in the way described in order to facilitate the measurements of their spectro-temporal features.

Despite the preprocessing of the waterfalls there are still several tasks that are needed on a burst-by-burst basis, that, with a large number of bursts and measurements to manage, can quickly become overwhelming and difficult to review. These tasks include additional noise removal, additional subsampling to increase the S/N, and separating the components of bursts with multiple pulses. While these tasks can be automated to an extent, being able to manage and customize a measurement allows for more accurate results and the inclusion of strange bursts that might not fit in an automation pipeline of limited complexity. To this end we developed an extensible graphical user interface (GUI) called Frbgui that allows a user to input additional masks, change the subsampling of the data, and isolate components of a burst, and used it to prepare bursts and obtain measurements of the spectro-temporal features.

The spectro-temporal features of burst each are obtained via a 2D Gaussian fit to the 2D autocorrelation of the burst waterfall. An autocorrelation of the waterfall helps increase the S/N for measurement and limits the effect of spectral structures, noise, and banding in the burst and the Gaussian model of the autocorrelation provides an analytical and robust way of measuring the spectro-temporal features from a small number of parameters. This technique is detailed in Appendix A of Chamma et al. (2021) (for example), and for this study, the Gaussian fit is obtained using the physical coordinates of the autocorrelation. Thus, though the dimensions of the Gaussian model's parameters are unitless, the inputs are normalized by the units of the autocorrelation's axes and we obtain

$$G\left(\frac{x}{1\,\mathrm{ms}}, \frac{y}{1\,\mathrm{MHz}}\right) = C \exp\left\{-\frac{1}{2}\left[(x-x_0)^2\left(\frac{\cos^2\theta}{b^2}+\frac{\sin^2\theta}{a^2}\right)\right.\right.$$
$$+2(x-x_0)(y-y_0)\sin\theta\cos\theta\left(\frac{1}{b^2}-\frac{1}{a^2}\right)$$
$$\left.\left.+(y-y_0)^2\left(\frac{\sin^2\theta}{b^2}+\frac{\cos^2\theta}{a^2}\right)\right]\right\}, \quad (1)$$

[2] https://github.com/mtlam/PyPulse
[3] https://github.com/thepetabyteproject/your
[4] https://thepetabyteproject.github.io/burstfit/

where C, x_0, y_0, a, b, and θ are the model parameters corresponding to the amplitude, central x- and y- positions, the standard deviations of the Gaussian, and the orientation of the semi-major axis (a) measured from counterclockwise from the positive y-axis. The fit is found using the `scipy.optimize.curve_fit` package and we found that the use of physical coordinates when obtaining this fit improves the accuracy of the sub-burst slope measurements by almost 40% when the burst is nearly vertical. The sub-burst slope and burst duration are obtained via equations A2-A3 of Chamma et al. (2021), with the modification that the unit conversion becomes unity due to the choice of coordinates when obtaining the Gaussian fit, so that

$$\frac{d\nu_{\rm obs}}{dt_{\rm D}} = -\left(1\ \frac{\rm MHz}{\rm ms}\right)\cot\theta, \tag{2}$$

$$t_{\rm w} = (1\ {\rm ms})\ \frac{ab}{\sqrt{b^2\sin^2\theta + a^2\cos^2\theta}}, \tag{3}$$

where $d\nu_{\rm obs}/dt_{\rm D}$ and $t_{\rm w}$ are the sub-burst slope and sub-burst duration[5], respectively, and $\nu_{\rm obs}$ and $t_{\rm D}$ are the frequency and delay time (or arrival time) of the burst, written in the formalism of Rajabi et al. (2020). We also compute the total bandwidth $B_{\rm tot}$ according to

$$B_{\rm tot} = (1\ {\rm MHz})\ 2\sqrt{2\ln 2}a\cos\theta, \tag{4}$$

which is the semi-major axis of the Gaussian ellipsoid scaled to its full-width-half-max value and projected on to the frequency axis. Figure 2 shows an example measurement of the spectro-temporal properties of burst B006 from Aggarwal et al. (2021). Numerically, equation (2) is equivalent to finding the line that connects the peaks of each row of the autocorrelation and finding the corresponding slope, while equation (3) is equivalent (up to a factor of $2\sqrt{\ln 2}$) to finding the FWHM of the 1D autocorrelation at a frequency lag of zero. For bursts with multiple components in a single waterfall, the autocorrelation changes in size to include the multiple components and equations (2) to (4) are still valid. We can therefore perform the same analysis to obtain the drift rate if a fit can be found to the larger autocorrelation. The drift rates we obtain are treated distinctly from the sub-burst slopes as these potentially arise from different phenomena.

Because the choice of DM affects the value of the sub-burst slope and, to a lesser extent, the sub-burst duration, each burst is measured over a range of trial DMs. The DM varies from burst to burst and for a single burst, especially unresolved pulses, the DM might be ambiguous if it is unclear whether to maximize the S/N of the burst or its structure (Gajjar et al. 2018; Chamma et al. 2021, Sec 2.1). We therefore measure each burst over a grid of DMs spanning 555 to 575 pc/cm^3 in steps of 0.5 pc/cm^3, chosen to account for the historical range of DMs observed from FRB20121102A. Each burst is incoherently dedispersed from its reported DM to the trial DM and measured via autocorrelation, resulting in 42 sets of measurements per burst including the reported burst DM. The total set of measurements obtained over the DM grid are then filtered to exclude sub-burst slopes that are positive or with fitting errors larger than 40%. We exclude all positive sub-burst slopes under the assumption that they are unphysical and due to over dedispersion (Chamma et al. 2021; Jahns et al. 2022). The remaining measurements are then grouped by DM and a fit is found between the sub-burst slope and duration of the form $A/t_{\rm w}$, which is the relationship predicted for these two properties by the relativistic dynamical model (Rajabi et al. 2020). Of this set of fits, we compute a reduced-χ^2 to assess the goodness of the fit and tabulate the remaining number of bursts for each DM, ie., the number of bursts that passed the filtering process. For each of the datasets listed in Section 2, the range of DMs is limited to only include those DMs that include all the bursts in the sample, and, within this limited range, the DM with optimal (minimal) reduced-χ^2 is chosen as the representative DM for that sample. The range of values in the remaining measurements in the limited DM range are then used as an estimate of the uncertainties. For example, the bursts from Michilli et al. (2018) are measured over the DM range 555-575 pc/cm^3, and, after filtering invalid measurements, the remaining DMs that include all of the bursts range from 555-560 pc/cm^3. Within this limited DM range, the DM with optimal reduced-χ^2 is found to be 558 pc/cm^3, and the range of measurements over the limited DM range are used as the uncertainties of the measurement at 558 pc/cm^3. Treating the measurements of each burst in this manner helps account for the effect of the DM on the measurement and allows for an estimate of the uncertainties beyond those from the Gaussian model.

The measurements are reviewed visually with the help of the bars and slope indicators such as those shown on both panels of Figure 2. Plots of all measurements can be found online at XXX.

4 RESULTS

We describe the results of the autocorrelation analysis, the measurement filtering process, and the relationships between the spectro-temporal properties in this section. The sub-burst slope (normalized by the observing frequency) vs sub-burst duration is shown in Figure 3. Figures 4 and 5 show different correlations between the measured spectro-temporal properties, including the sub-burst duration and sub-burst slope with frequency, and in particular the correlations between the bandwidth with frequency, duration and sub-burst slope. We find an unexpected correlation between the bandwidth and duration (and thus sub-burst slope). In Figure 6, we look at the small sample of bursts with multiple components and show the drift rate vs duration and drift rate vs. frequency, and finally we look in particular at the bursts from Li et al. (2021) in Figure 7 and the lack of differences in the spectro-temporal features between bursts from the different energy and wait-time peaks.

As mentioned in the previous section, the measurements are filtered to exclude invalid values and this process results in some bursts not having a valid measurement at a particular DM, which results in a limited DM range after requiring that all bursts are included. After this filtering, the ranges of DMs for which bursts have valid measurement varied from dataset to dataset; while all five datasets had valid measurements down to 555 pc/cm^3, the highest DMs at which all bursts in a dataset still had valid measurements differed. These maximal DMs along with the DM in that range that had the optimal fit between the sub-burst slope and duration are listed in Table 1. The average maximal DM (weighted by the number of bursts in each dataset) was 561.5(4) pc/cm^3 and the average optimal DM was 560.1(8) pc/cm^3. In the figures to follow, burst measurements are always displayed at the optimal DM of the dataset they come from, with uncertainties estimated from the range of measurements found within the limited DM range.

[5] The duration defined in eq. (3) is the correlation length of the burst, and can be converted to other definitions of burst duration with a simple scaling. If the burst is Gaussian with a standard deviation of $\sigma_{\rm p}$ and FWHM $t_{\rm FWHM} = 2\sqrt{2\ln 2}\sigma_{\rm p}$, then the correlation length $t_{\rm w}$ is related to those durations by $t_{\rm w} = \sqrt{2}\,\sigma_{\rm p}$, and $t_{\rm w} = 1/\sqrt{4\ln 2}\,t_{\rm FWHM} \simeq 0.6\,t_{\rm FWHM}$.

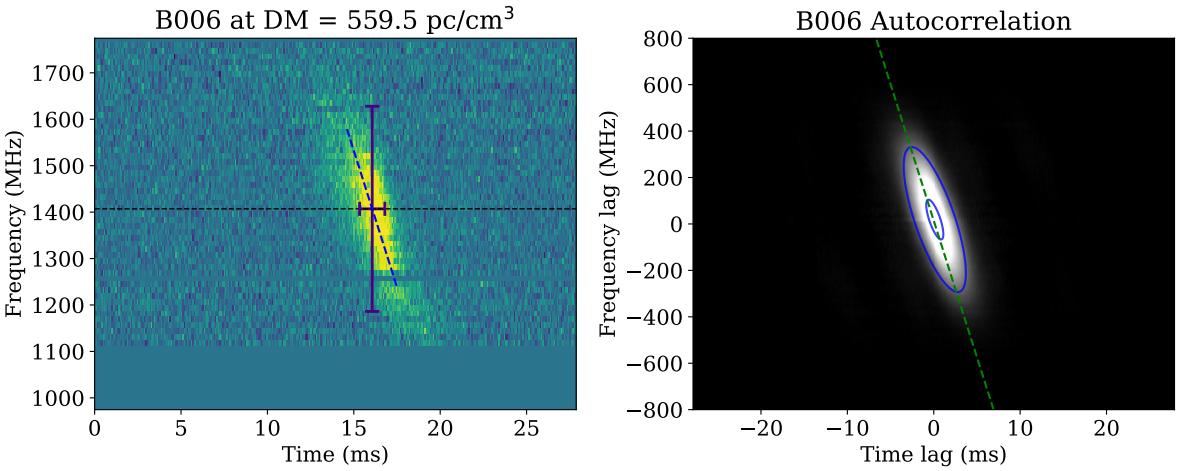

Figure 2. Example measurement of burst B006 from Aggarwal et al. (2021). The left panel shows the burst waterfall dedispersed to 559.5 pc/cm^3 with the dashed line, horizontal bar, and vertical bar indicating the sub-burst slope, duration, and total bandwidth obtained via the 2D Gaussian model of the autocorrelation, shown on the right. On the right, the image shows the computed autocorrelation, and the blue outlines are contours of the Gaussian model at a quarter and 90% of the peak. The dashed green line shows the corresponding slope.

Dataset	Max valid DM (pc/cm^3)	Optimal DM (pc/cm^3)	# of bursts
Michilli et al. (2018)	560.0	558.0	19
Gajjar et al. (2018)	563.5	557.5	21
Oostrum et al. (2020)	563.0	563.0	23
Aggarwal et al. (2021)	560.5	559.5	63
Li et al. (2021)	562.0	562.0	42
Weighted Average:	561.5(4)	560.1(8)	168

Table 1. Results from the measurement exclusion and DM optimization process described in Section 3. The max valid DM is the DM at which bursts start being excluded for having invalid sub-burst slope measurements (ie. being over-dedispersed). The optimal DM is the DM for which the reduced-χ^2 of the fit between the sub-burst slope and duration measurements at that DM is minimal. The DM step size used was 0.5 pc/cm^3.

4.1 Spectro-temporal Properties

The correlations between the spectro-temporal properties shown in Figures 3 to 5 confirm known relationships across a broader parameter range and reveal a new relationship between the bandwidth and sub-burst duration (or sub-burst slope). In Figure 3 we plot the sub-burst slope normalized by the observing frequency versus the sub-burst duration. We find three fits to the data using the `scipy.odr` package, which performs an orthogonal distance regression, a method that takes into account the errors on both variables. The first fit is of the form $A\,t_{\rm w}^{-1}$ and we find $A = 0.113 \pm 0.003$, and the more general fits to $A\,t_{\rm w}^{n}$ and $A\,t_{\rm w}^{n} + B$ yield $A = 0.110 \pm 0.003$, $n = -0.81$ and $A = 0.046 \pm 0.003$, $n = -1.25$, $B = 0.015{\rm ms}^{-1}$. For each dataset, a range of fits of the form $A\,t_{\rm w}^{-1}$ is found over the DM range and the shaded region plotted shows the intersection of those ranges across the five datasets. That is, the shaded region shows the range of fits possible within the limited DM ranges of all the datasets and is an estimate of the uncertainty on the parameter A as a function of the DM. We see that a majority of points fall within this region and are well described by the fits, with a small population of outliers that lie above the rest of the points in the sub-bursts with durations greater than 1 ms. In Figure 4, we plot the sub-burst duration, sub-burst slope and sub-burst slope normalized by $\nu_{\rm obs}^2$ each against the frequency. In those three panels, the black line represents a fit of the form with the exponent fixed to the prediction by the relativistic dynamical model Rajabi et al. (2020) and the tan line represents a fit where the exponent is unfixed. In the sub-burst duration vs. frequency plot, the free fit finds an exponent of $n = -0.870$, smaller than the predicted $n = -1$, and in the slope vs. frequency plot we find $n = 1.749$, also smaller than the predicted $n = 2$ relationship. Both fits visually describe the data well, and we see a large spread in the bursts in all three plots. In the third panel, a general power law fit finds $n = 0$, or a constant value, which is exactly the relationship predicted. The constant found is $B = 4.28 \times 10^{-8}$. In Figure 5 we plot three correlations between the sub-burst bandwidth and the, respectively, frequency, sub-burst duration, and sub-burst slope. We find a general fit to the bandwidth vs. frequency, and this yields a fit with exponent $n = 0.86$, and $A = 0.45 \pm 0.15$. We also fit a linear fit with exponent fixed to $n = 1$ and find a slope of $A = 0.14 \pm 0.004$. For the fits to the sub-burst duration and slope, we leave the exponent free and find $A = 404 \pm 11$ and $n = -0.38$ for the duration and $A = 41 \pm 8$ and $n = 0.44$ for the sub-burst slope. That these exponents are almost inverses of each other is expected from the inverse trend between the slope and duration shown in Figure 3, but the fact that there is a relationship between the bandwidth and slope/duration at all is surprising, and may be seen in this data because of the large range in frequency of the bursts sampled. However, as shown by the bandwidth limits plotted as horizontal lines in the figures, the maximum observable bandwidths for the Oostrum et al. (2020), Aggarwal et al. (2021), and Li et al. (2021) datasets are 200 MHz, 680 MHz, and 500 MHz respectively due to their telescopes (with a few exceptions for bursts that had slightly different backends). These bandwidth limits do not explain the dearth of low bandwidth bursts from the high frequency and higher bandwidth datasets. The nearest fractional value for an exponent of $n = 0.44$ is about 2/5 and so these two plots, if observationally complete, suggest a proportionality of $B_\nu \propto t_{\rm w}^{-2/5} \propto (d\nu_{\rm obs}/dt_{\rm D})^{2/5}$, where B_ν is the bandwidth.

The correlations shown here provide evidence that the relationships between the sub-burst duration, slope and frequency apply for a majority of bursts from this source and possibly indicate an additional relationship between the bandwidth and sub-burst slope/duration.

The drift rate of a burst with multiple components may be due to a different phenomena than that that results in the sub-burst slope, and so we separate the drift rate measurements from the sub-burst slope measurements and show their correlations in Figure 6, seeing that their relationships are similar to those found for the sub-burst slopes. Of our sampled bursts only a handful showed multiple components. Most of these were measurable via autocorrelation but a few were not, such as in the cases where one of the bursts dominated the autocorrelation or when the drift rate was very small. The drift rates are put through the same filtering process as the sub-burst slopes and the left panel of Figure 6 shows the normalized drift rate vs. the duration of the event, while the right shows the drift rate vs. the frequency. As before, for the relationship with the duration we find one fit with the exponent fixed to $n = -1$ which yielded $A = 0.145 \pm 0.012$ and a fit with a free exponent which yielded $A = 0.119 \pm 0.012$ and $n = -0.71$. This first fit has an A value higher than that found for the sub-burst slopes and outside the range of fits shown in Figure 3 while the second fit found a slightly lower exponent. For the relationship with the frequency we perform two fits as well and the first fit with exponent fixed to $n = 2$ yielded $A = (4.7 \pm 0.7) \times 10^{-5}$, which is equivalent within uncertainties to the value found between the slope and frequency (shown in the middle panel of Figure 4), and the fit with the free exponent found $A = (0.004 \pm 0.004)$ and $n = 1.375$, a nearly linear fit, however with quite a large error on A. For the limited drift rates available, the fits to the drift rates' relationships are similar enough to those found for the sub-burst slopes that it is hard to conclude if these differences are significant or if the same relationships might describe both phenomena.

For the sampled bursts from the bimodal peaks in energy and wait-time distributions reported by Li et al. (2021), we searched for correlations between our measured spectro-temporal properties and the burst energy and wait-time, finding that they were unrelated to each other. Figure 7 shows plots of the slope, sub-burst duration, bandwidth, and frequency as functions of the wait-time (top row) and burst energy (bottom row). In the top row we can see that the bursts cluster around wait-times of 10^{-2} and 10^{2} seconds, corresponding to the two sampled peaks, and that the spectro-temporal measurements in all panels vary randomly and with similar ranges. In the bottom row a large number of bursts cluster around 10^{39} erg while the low energy peak at $< 10^{38}$ erg only has two points, due to difficulties we encountered in measuring these lower S/N bursts. Nonetheless, across the four panels we again see that the measurements vary widely at the high energy peak and cover similar values as the measurements from the low energy peak. For this sample of data we therefore conclude that no clear relationship exists between the wait-time and energy of a burst with any of its spectro-temporal properties.

We have presented here new measurements of the spectro-temporal properties of bursts sampled from five studies of FRB20121102A and characterized the relationships, and lack of relationships, between them. Across this broad sample we saw that the sub-burst slope and sub-burst duration are approximately inversely related, shown in Figure 3, that the sub-burst duration and frequency are also inversely related, that the slope goes approximately to the square of the frequency, and that the bandwidth varies linearly with the frequency. We also tentatively found a relationship between the bandwidth and sub-burst duration with a proportionality of nearly $t_{\rm w}^{-2/5}$. Because of the inverse relationship between the duration and sub-burst slope, we therefore expect a relationship between the bandwidth and slope that goes nearly as $(d\nu_{\rm obs}/dt_{\rm D})^{2/5}$, and this is exactly what is seen in the bottom panel of Figure 5. We also looked at a handful of drift rates in our sample separately from measurements of the sub-burst slope and found similar but not identical relationships as those found for the sub-burst slope. Due to the low statistics it is unclear whether different relationships describe the sub-burst slope and drift rate or if they are identical, but nonetheless the relationships between the two are certainly difficult to distinguish. Finally, by looking at bursts sampled from the bimodal energy and wait-time distributions reported by Li et al. (2021), we see no connection between those two parameters and the subsequent spectro-temporal properties of a burst.

5 DISCUSSION

We discuss here our results in the context of other studies, the spectro-temporal relationships found and their context in the relativistic dynamical model (Rajabi et al. 2020), and the expected relationship for the drift rates as compared to that for the sub-burst slopes. We will also discuss the implications of the relationships observed and not observed in the case of the spectro-temporal properties with the burst energy and wait time, the large spread in values seen in the measurements of the spectro-temporal properties, and what these mean about understanding FRBs overall.

Several studies have now closely examined the relationships between spectro-temporal properties of FRBs and found strong correlations between them, especially between the sub-burst slope and sub-burst duration. The first report of the inverse relationship between the slope and duration was in Rajabi et al. (2020), seen with 25 bursts from FRB20121102A and Chamma et al. (2021) first reported the same relationship for multiple sources seen with bursts from, in addition to FRB20121102A, FRB20180916B and FRB20180814A, and also reporting that the same fit parameter A characterized the relationship for the three sources. In earlier work the data for FRB20121102A was limited to bursts with short durations and frequencies greater than 4 GHz, and since then large numbers of bursts were made available at longer durations and lower frequencies, presenting the opportunity to understand the relationships seen earlier with improved statistics. In this study the frequency range, duration range are broader and the number of bursts studied from FRB20121102A is more than six-fold larger and we see a majority of bursts follow a tight relationship. The fit parameter found here was $A = 0.113 \pm 0.003$, which is higher than the $A = 0.078 \pm 0.006$ found by Chamma et al. (2021), along with a narrower range of fits centered around $A = 0.09$. Though the range of fits includes this earlier value, the low frequency bursts added in this study exhibit a small population of outliers that are found higher than the fit region, which may be responsible for the larger A value found here. Based on the uncertainty ranges, this population can be seen to be near the edge of its limited DM range, meaning the bursts are near vertical where errors on the slope measurement are large and close to being over-dedispersed. In Jahns et al. (2022), 849 bursts from FRB20121102A are analysed on the lower end of the frequency range (around 1400 MHz) and a strong inverse correlation between the sub-burst duration and slope can be seen in their Figure 5. Their formalism finds the inverse of the sub-burst slope relation used here and their fit parameter of $|b| = 0.00862(37)$ MHz^{-1} can be converted to the results here for comparison via $A = 1/\nu_{\rm obs} b$, which yields $A_{\rm Jahns} = 0.0839$ when using $\nu_{\rm obs} = 1400$ MHz, the most common burst frequency in that sample. This value is comparable to the results found here, and differences can be due to the burst definition used and details of the analysis (such as normalizing each point by

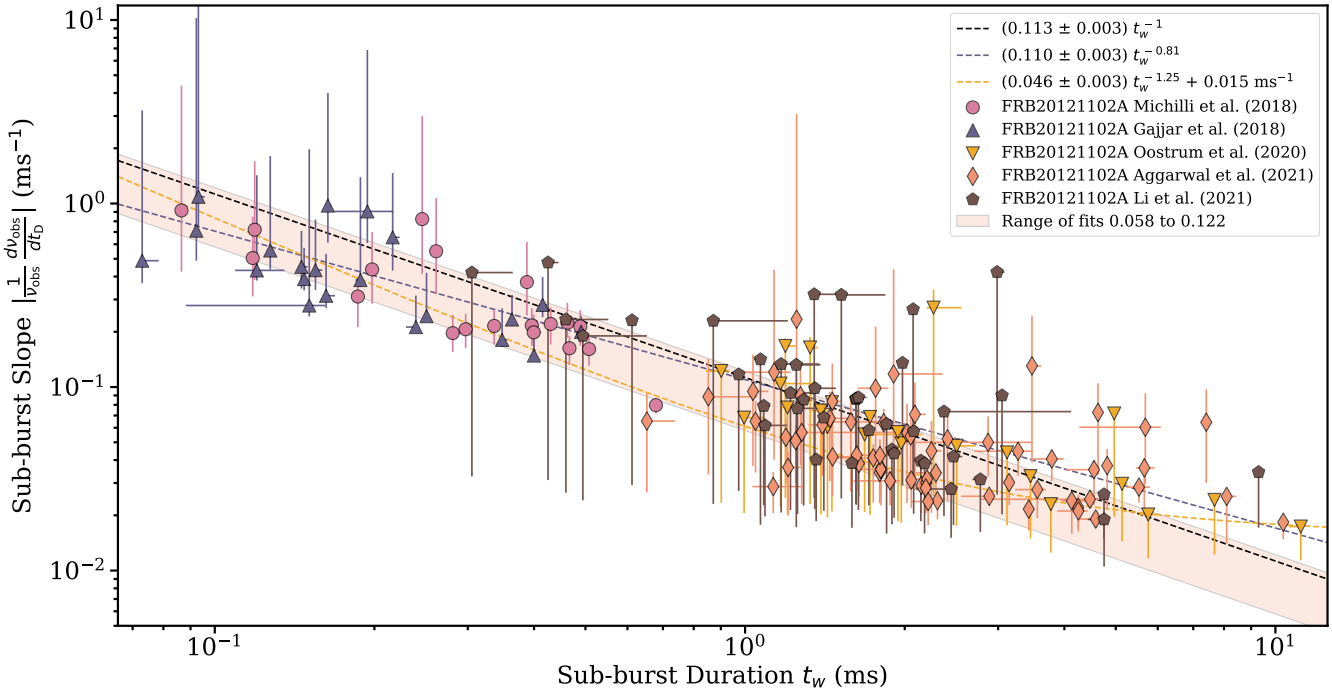

Figure 3. The relationship between the sub-burst slope and sub-burst duration. The sub-burst slope is normalized by the burst frequency in order for the different datasets to be plotted together with the same relationship. The black line is a fit of the form $A\,t_w^{-1}$ which is the relationship predicted in the relativistic dynamical model, while the other are more general fits of the form $A\,t_w^n$ and $A\,t_w^n + B$. The shaded region shows the intersection of the range of fits found over the DM ranges of each of the five datasets. Each measurement is displayed at the optimal DM for its source dataset, listed in Table 1. We see decent agreement between the three fits with the exponent of the expected relation lying between those found for the general fits.

the burst frequency). In Houde et al. (2019), the linear relationship shown in the top panel of Figure 5 between bandwidth and frequency is seen in their Figure 5, and includes points between 2 and 4 GHz.

Other relationships are more difficult to see with a narrow range of frequencies and durations, such as the near inverse relationship between sub-burst duration and frequency, and near quadratic relationship between slope and frequency, shown in the first two panels of Figure 4. The relativistic dynamical model Rajabi et al. (2020) predicts the relationship between the sub-burst duration and frequency to be

$$t_{\rm w} = \tau'_{\rm w}\frac{\nu_0}{\nu_{\rm obs}}, \tag{5}$$

where $t_{\rm w}$ is the sub-burst duration, $\tau'_{\rm w}$ is the sub-burst duration in the rest frame of emission, ν_0 is the rest frame frequency, and $\nu_{\rm obs}$ is the frequency in the observer frame. The values of $\tau'_{\rm w}$ and ν_0 can be absorbed into a constant and so a simple inverse relationship is expected, and this relation arises simply from the Lorentz transformation of the space-time coordinates in the FRB frame to the observer's frame. The authors are not currently aware of other evidence of this relationship and this may be due to the fact that it is only apparent across the entire observed frequency range of FRB20121102A. Each 'clump' of bursts seen in Figure 4 viewed independently appears uncorrelated with the observing frequency, but placed together a downward trend becomes clear. The relationship between sub-burst slope and frequency is similar in this regard as well, since over a narrow spectral range the two observables appear uncorrelated, but Wang et al. (2022) in their Figure 8, using data from multiple studies and multiple FRB sources and spanning a large frequency range found that trends proportional to ν^2 and $\nu^{2.29}$ fit the data well. Our results showed similar relationships fit well, though our free exponent fit found a lower value of $\nu^{1.749}$. The relationship between the sub-burst slope and frequency can be derived from the relativistic dynamical model Rajabi et al. (2020) using equation (5) and the relationship between the sub-burst slope and duration, which is

$$\frac{1}{\nu_{\rm obs}}\frac{d\nu_{\rm obs}}{dt_{\rm D}} = -\left(\frac{\tau'_{\rm w}}{\tau'_{\rm D}}\right)\frac{1}{t_{\rm w}} = -\frac{A}{t_{\rm w}}, \tag{6}$$

where as before $\frac{d\nu_{\rm obs}}{dt_{\rm D}}$ is the sub-burst slope, $t_{\rm D}$ is the delay time (or arrival time), and $\tau'_{\rm D}$ is the delay time in the rest frame of the FRB. The fit parameter A is seen here as the ratio between the rest frame sub-burst duration and delay time, and this relationship is the one predicted for the sub-burst slope and duration, shown with the black fit in Figure 3. Combining equations (5) and (6) we obtain

$$\frac{d\nu_{\rm obs}}{dt_{\rm D}} = -\frac{A\nu^2_{\rm obs}}{\tau'_{\rm w}\nu_0} = -A'\nu^2_{\rm obs}, \tag{7}$$

where the new constant $A' = A/\tau'_{\rm w}\nu_0 = 1/\tau'_{\rm D}\nu_0$. This is a quadratic relationship between the sub-burst slope and frequency and is by our results and the results of Wang et al. (2022). Interestingly, if there is a way to estimate the rest frame sub-burst duration $\tau'_{\rm w}$, then the ratio of A and A' would provide a measure of the rest frame frequency of emission ν_0, through

$$\frac{A}{A'} = \nu_0\tau'_{\rm w}. \tag{8}$$

These relationships of the sub-burst slope and duration with frequency are difficult to characterize without a large range of observations, but if that data is available such as with FRB20121102A,

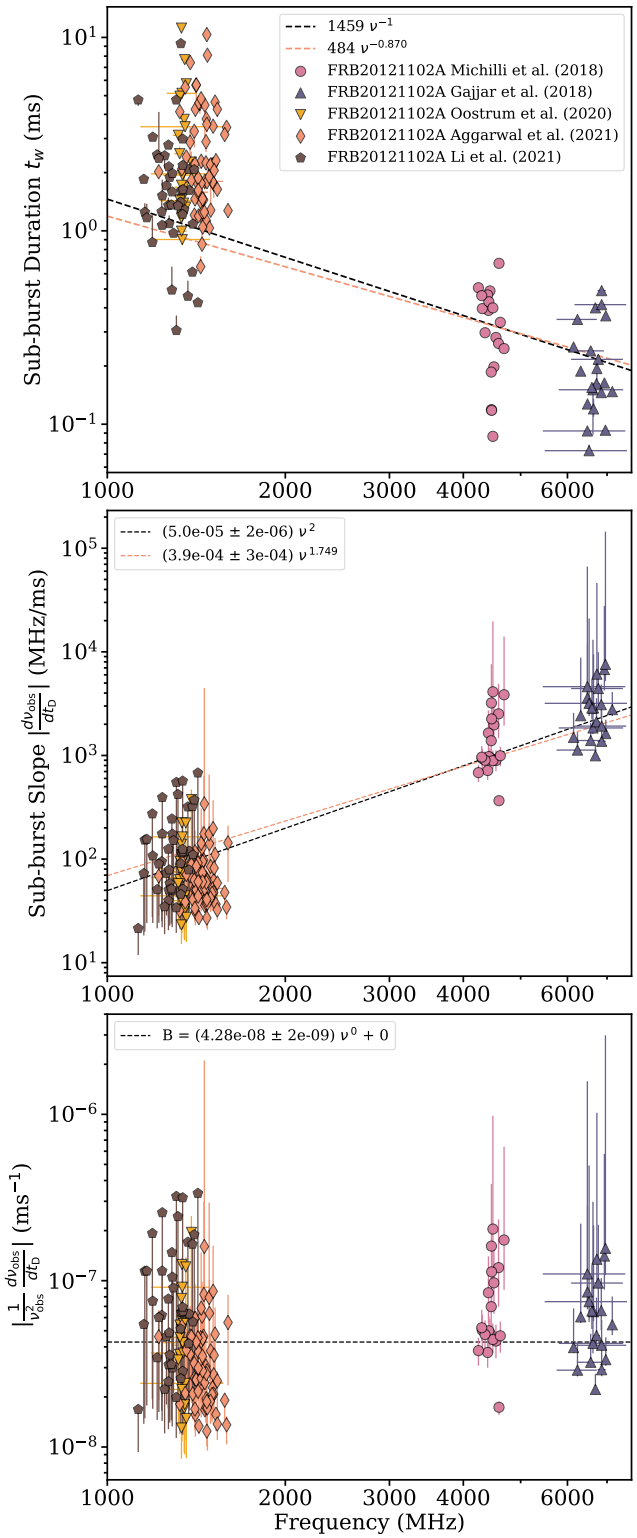

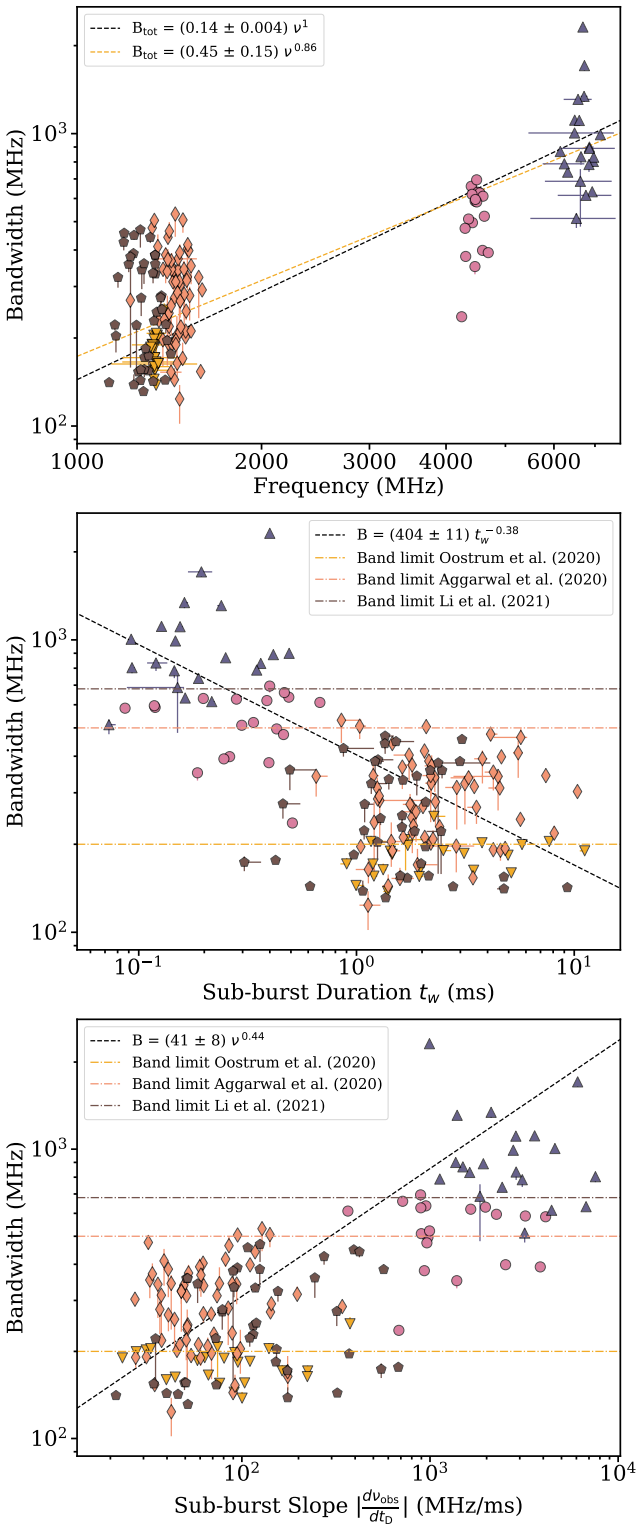

Figure 4. Relationships between the sub-burst duration (top), the sub-burst slope (middle) and the sub-burst slope over ν_{obs}^2 (bottom) with burst frequency. Colors for all are shown in the top panel and are the same as in Figure 3. In the top and middle panels, the black line shows a fit to the relationship predicted by the triggered dynamical model in Rajabi et al. (2020), and the tan lines are general fits of the form Ax^n. For the bottom panel a constant value is predicted and the black line is a general power law fit that found a constant value.

Figure 5. Relationships between the bandwidth and the burst frequency (top), sub-burst duration (middle) and sub-burst slope (bottom). The relationship between the bandwidth and frequency is linear, while the relationship with the duration goes nearly to the power of −2/5. The origin of this relationship is unclear, and may be due to observational bias as indicated by the overlayed lines showing the bandwidth limits. In the bottom panel we see that the fit found between the bandwidth and slope is nearly the inverse of that for the duration, as might be expected based on the inverse relationship shown in Figure 3.

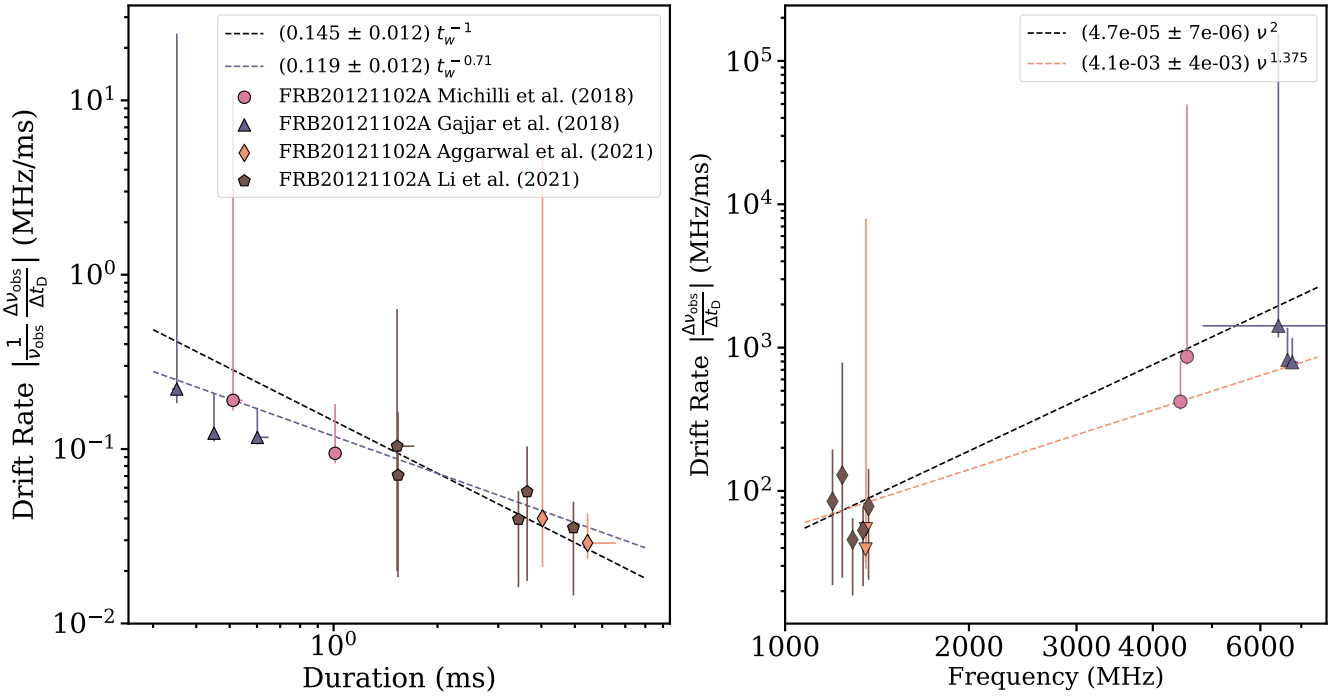

Figure 6. Relationships between the drift rate of multiple components and the duration (left) and the frequency of observation (right). On the left, fits of the form $A\,t_w^{-1}$ and $A\,t_w^{n}$ are made for comparison with the similar inverse relationship between the sub-burst slope and duration shown in Figure 3. On the right, we find two fits with one locked to a power of 2 and the other allowed to change, resulting in a nearly linear fit.

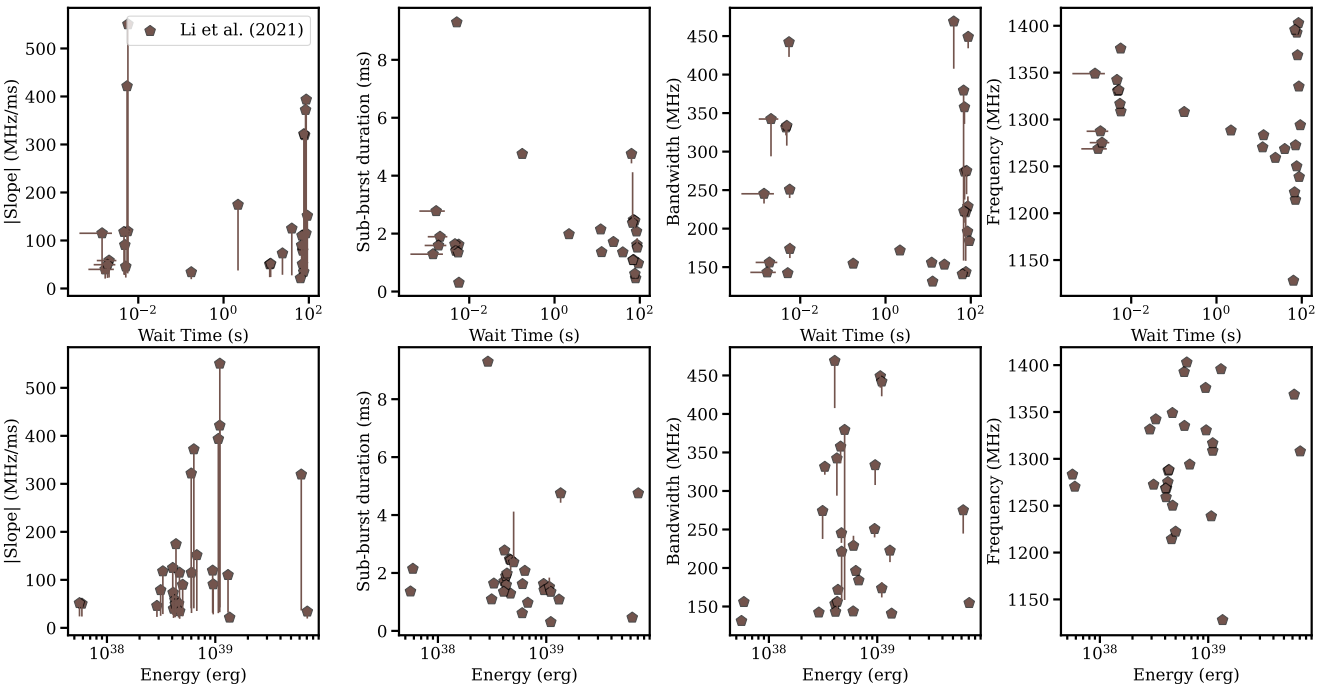

Figure 7. Correlations between measured spectro-temporal properties of bursts from Li et al. (2021) and their wait-times (top) and energies (bottom), as reported by those authors. The two peaks of the wait-time distributions can be seen in the top row around 10^{-2} and 10^{2} seconds. The two peaks of the energy distribution are less obvious due to difficulties measuring bursts from the low energy ($<10^{38}$ erg) peak. No obvious relationship of a burst's spectro-temporal properties on either its wait time or energy is seen in this data.

they serve as useful tools especially in the context of the relativistic dynamical model.

The drift rate relationships with duration and frequency are plotted in Figure 6 and these relationships appear to be analogous relationships with the relationships that exist for the sub-burst slope. For the limited data available, the drift rate relationship with frequency seems to be adequately described by the fit proportional to ν^2 and the free fit proportional $\nu^{1.375}$, which is closer to linear than not. We can derive a relationship between the drift rate and the frequency using equation 8 of Rajabi et al. (2020) which describes the change in frequency with arrival time of distinct sub-bursts. Expanding the $d\nu_{\rm obs}/d\tau'_{\rm D}$ term in that equation we get

$$\frac{\Delta\nu_{\rm obs}}{\Delta t_{\rm D}} = \frac{\nu_{\rm obs}}{\nu_0}\frac{d\nu_{\rm obs}}{d\tau'_{\rm D}} = \frac{\nu_{\rm obs}}{\nu_0}\frac{d\nu_{\rm obs}}{d\beta}\frac{d\beta}{d\tau'_{\rm D}}, \tag{9}$$

where β is the fraction of the speed of light the FRB source is moving with along the line of sight. By using the relativistic Doppler shift formula $\nu_{\rm obs} = \nu_0\sqrt{(1+\beta)/(1-\beta)}$, we can evaluate $d\nu_{\rm obs}/d\beta$ in the above expression to obtain

$$\frac{\Delta\nu_{\rm obs}}{\Delta t_{\rm D}} = \frac{\nu^2_{\rm obs}}{\gamma^2\nu_0}\frac{d\beta}{d\tau'_{\rm D}}, \tag{10}$$

where $\gamma = 1/\sqrt{1-\beta^2}$. Equation (10) shows a ν^2 dependence with the frequency, however, equivalently we could infer a linear relationship if the $d\nu_{\rm obs}/d\tau'_{\rm D}$ term, which is a parameter of the environment, turns out to be constant. More data is required to verify which relationship is correct, and that result can be interpreted within the model based on the relations described above. For the relationship between the drift rate and the duration of the even, it is not clear how one can derive such a relationship except in terms of $\Delta t_{\rm D}$, but the data seems to suggest an inverse relationship analogous to the relationship between the sub-burst slope and sub-burst duration.

There is no known relationship within the relativistic dynamical model that explains the approximately $t_{\rm w}^{-2/5}$ relationship seen between the bandwidth and the sub-burst duration, and conversely, the $(d\nu_{\rm obs}/dt_{\rm D})^{2/5}$ relationship between the bandwidth and sub-burst slope.

5.1 Spectro-temporal properties and their relationship to the emission process

Across the different relationships explored and for the broad sample of bursts considered from FRB20121102A, there does not seem to be a large population of outliers that breaks sharply from the relationships described, which, in light of the lack of correlations between the spectro-temporal properties and the energy and wait-time, allows us to uncouple the spectro-temporal properties of an FRB from its emission process. This is because the simplest explanation for the lack of outliers or bursts classified by the trend their spectro-temporal properties follow is that the correlations between the spectro-temporal properties of FRBs (at least from this source) originate from a single phenomenon, and their good agreement with the relativistic dynamical model implies that the single phenomenon that gives rise to the observed spectro-temporal correlations is relativity and the Lorentz transformation. For a source to be subject to relativity and give rise to the correlations seen here it must be made of material that moves such as ions or electrons, as opposed to a source that only consists of an electric or magnetic field. Disturbances in such fields can certainly give rise to motions in a material that then emits the FRB, but the results presented here strongly suggest that all FRB emission from this source comes from material that is moving very quickly, and that all spectro-temporal correlations of a FRB20121102A are completely determined by the dynamics of that material, and not due to the actual emission process. This is supported by the results shown in Figure 7, where several spectro-temporal properties appear uncorrelated with both the wait-time and energy of a burst, and also by the correlations with energy displayed in Figure 5 of Jahns et al. (2022) for bursts around 1400 MHz, the relationship between the frequency and flux density shown in Figure 4 of Gajjar et al. (2018) for bursts around 7 GHz, and correlations with the fluence shown in Figure 5 of Aggarwal et al. (2021) for bursts around 1400 MHz. These aforementioned correlations are done independently over a narrow range of frequencies and durations, and an analysis with a broad sample such as the one used for this study that focuses on the energy and/or fluxes of bursts would be needed to reinforce the separation of the spectro-temporal relationships from the emission process, as the present results suggest.

While there is a lack of bursts that sharply contrasts with the spectro-temporal relationships found, there is considerable spread in the values of sub-burst slope, duration and bandwidth seen in Figures 3 to 5 for relatively narrow range in frequency that appears to be related to the emission process. For example, the data for Michilli et al. (2018) cluster around 4.5 GHz, but values for the sub-burst slope range from 5×10^2 MHz/ms to 4×10^3 MHz/ms, and the sub-burst duration spans nearly an order of magnitude. Similar statements are true for all the other datasets considered. In the relativistic dynamical model the sub-burst duration and sub-burst slope (see equations 5 and 6) are related to the rest frame frequency ν_0, and the rest frame duration and delay times $\tau'_{\rm w}$ and $\tau'_{\rm D}$. The dependence of the sub-burst duration and slope on these properties, which are determined exclusively by the emission process including the FRB environment, is possibly the cause of the dispersion seen in the spectro-temporal properties. Characterizing the dispersion of spectro-temporal properties for large samples of bursts may therefore be an avenue for studying the emission process.

6 CONCLUSIONS

We studied the spectro-temporal properties and the relationships between them of a broad sample of 168 bursts from FRB20121102A with frequencies ranging from 1 to 7.5 GHz and sub-burst durations ranging from less than 1 ms to about 10 ms from the observational studies of Michilli et al. (2018), Gajjar et al. (2018), Oostrum et al. (2020), Aggarwal et al. (2021), and Li et al. (2021). In the latter study, we sampled bursts from the two peaks of the bimodal energy distribution and bimodal wait-time distribution reported therein in order to search for relationships between those parameters and the spectro-temporal properties of the bursts. Our measurements of the spectro-temporal properties include measurements of the sub-burst slope, sub-burst duration, burst bandwidth, center frequency, and sad trombone drift rate (when applicable) at each DM between 555 to 575 pc/cm^3 in steps of 0.5 pc/cm^3. The complete set of measurements are available online along with an extensible graphical user interface called Frbgui that was developed and used to prepare and perform measurements on the burst waterfalls.

We characterized multiple relationships between the measured spectro-temporal properties of bursts from FRB20121102A finding general agreement with multiple predictions from the relativistic dynamical model described in Rajabi et al. (2020). We found, as in earlier works, an inverse relationship between the sub-burst slope and sub-burst duration, as well as an inverse relation between the sub-burst duration and frequency, an approximately quadratic relation

between the sub-burst slope and frequency, and a linear relationship between the sub-burst bandwidth and frequency. We also found a correlation with power-law index near −2/5 between the sub-burst bandwidth and sub-burst duration, and because of the inverse relationship between the sub-burst slope and duration, a relationship between the bandwidth and slope with power-law index near 2/5. This relationship is unexplained and is potentially due to the limited observing bands at lower frequencies, however this would not explain the lack of small bandwidth bursts observed at high frequencies. The 12 drift rates measured were seen to follow relationships with the duration and frequency that are analogous to the ones obeyed by the sub-burst slope, however more data is needed to properly characterize these trends. We also searched for correlations between the spectro-temporal properties and the burst energy and wait times from the bimodal peaks reported in Li et al. (2021) and found that the spectro-temporal properties of a burst do not correlate with their energy or wait time, nor does the peak a burst comes from have an effect on the measured properties. Except for the bandwidth relationship, the multiple relationships observed between the spectro-temporal properties generally agree with the predictions made in Rajabi et al. (2020).

The general agreement of the spectro-temporal properties with the predictions of the relativistic dynamical model (Rajabi et al. 2020) from this broad sample of bursts from FRB20121102A suggests that the spectro-temporal properties of all bursts FRB20121102A are almost exclusively determined by dynamical motions of the FRB source, while the dispersion of values observed in the spectro-temporal properties seems to arise from the parameters in the model that are determined exclusively by the emission mechanism such as the rest frame frequency of emission and the rest frame timescales. Therefore, characterizing the dispersion of spectro-temporal properties from large samples of bursts may inform on the emission mechanism of FRBs.

ACKNOWLEDGEMENTS

We are grateful to Di Li for arranging access and support with the FAST data

DATA AVAILABILITY

All the measurements are available on github and the waterfalls can be obtained from the authors of their respective publications also check out my gui which is also on github

REFERENCES

Agarwal D., et al., 2020, Monthly Notices of the Royal Astronomical Society, 497, 352
Aggarwal K., 2021, The Astrophysical Journal Letters, 920, L18
Aggarwal K., Agarwal D., Lewis E. F., Anna-Thomas R., Tremblay J. C., Burke-Spolaor S., McLaughlin M. A., Lorimer D. R., 2021, The Astrophysical Journal, 922, 115
Anna-Thomas R., et al., 2022
Chamma M. A., Rajabi F., Wyenberg C. M., Mathews A., Houde M., 2021, Monthly Notices of the Royal Astronomical Society, 507, 246
Gajjar V., et al., 2018, The Astrophysical Journal, 863, 2
Gourdji K., Michilli D., Spitler L. G., Hessels J. W. T., Seymour A., Cordes J. M., Chatterjee S., 2019, The Astrophysical Journal, 877, L19
Hessels J. W. T., et al., 2019, The Astrophysical Journal, 876, L23
Houde M., Rajabi F., Gaensler B. M., Mathews A., Tranchant V., 2019, Monthly Notices of the Royal Astronomical Society, 482, 5492
Jahns J. N., et al., 2022
Josephy A., et al., 2019, The Astrophysical Journal, 882, L18
Li D., et al., 2021, Nature, 598, 267
Luo R., et al., 2020, Nature, 586, 693
Lyubarsky Y., 2021, Universe, 7, 56
Michilli D., et al., 2018, Nature, 553, 182
Nimmo K., et al., 2021
Nita G. M., Gary D. E., Hellbourg G., 2016, in 2016 Radio Frequency Interference (RFI). IEEE, doi:10.1109/rfint.2016.7833535
Oostrum L. C., et al., 2020, Astronomy & Astrophysics, 635, A61
Petroff E., Hessels J. W. T., Lorimer D. R., 2022, The Astronomy and Astrophysics Review, 30
Rajabi F., Chamma M. A., Wyenberg C. M., Mathews A., Houde M., 2020, Monthly Notices of the Royal Astronomical Society, 498, 4936
Wang W.-Y., Yang Y.-P., Niu C.-H., Xu R., Zhang B., 2022, The Astrophysical Journal, 927, 105

APPENDIX A: SOME EXTRA MATERIAL

If you want to present additional material which would interrupt the flow of the main paper, it can be placed in an Appendix which appears after the list of references.

This paper has been typeset from a TEX/LATEX file prepared by the author.